Surfaces, Interfaces, and Catalysis; Physical Properties of Nanomaterials and Materials

Dynamic Phase Diagram of Catalytic Surface of Hexagonal Boron Nitride in Conditions of Oxidative Dehydrogenation of Propane

Zisheng Zhang, Elisa Jimenez-Izal, Ive Hermans, and Anastassia N. Alexandrova

J. Phys. Chem. Lett., **Just Accepted Manuscript** • DOI: 10.1021/acs.jpclett.8b03373 • Publication Date (Web): 17 Dec 2018

Dynamic Phase Diagram of Catalytic Surface of Hexagonal Boron Nitride in Conditions of Oxidative Dehydrogenation of Propane

Zisheng Zhang[1,2], Elisa Jimenez-Izal[1,3], Ive Hermans,[4] Anastassia N. Alexandrova[1,5,*]

[1] Department of Chemistry and Biochemistry, University of California, Los Angeles, 607 Charles E. Young Drive, Los Angeles, California 90095-1569, United States

[2] Department of Chemistry, Southern University of Science and Technology, Shenzhen 518055, China

[3] Kimika Fakultatea, Euskal Herriko Unibertsitatea (UPV/EHU), and Donostia International Physics Center (DIPC), P. K. 1072, 20080 Donostia, Euskadi, Spain

[4] Department of Chemistry, University of Wisconsin-Madison, 1101 University Avenue, Madison, Wisconsin 53706, United States

[5] California NanoSystems Institute, Los Angeles, California 90095-1569, United States

*Corresponding Author e-mail: ana@chem.ucla.edu

Abstract. Partially oxidized surfaces of hexagonal boron nitride (hBN) and several metal borides are unexpectedly excellent catalysts for oxidative dehydrogenation of alkanes to olefins, but the nature of the active site(s) on these B-containing interfaces remains elusive. We characterize the surface of the partially oxidized B-rich hBN surface under reaction conditions from first principles. The interface has thermal access to multiple different stoichiometries, and multiple structures of each stoichiometry. The size of the thermal ensemble is composition-dependent. The phase diagram of the interface constructed on the basis of the statistical ensembles of many accessible states is very different from the one based on global minima. Phase boundaries shift and blur, and phases consist of several stoichiometries and structures. The BO-layer transiently exposes the reactive -B=O motifs in the metastable states. The fluxionality and structural diversity emerging at reaction conditions must be taken into account in theoretically descriptions of the catalytic interface.

TOC Graphics:

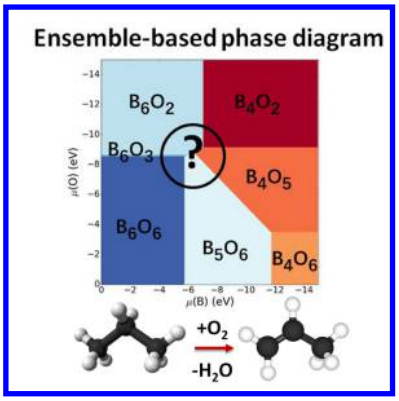

Propylene, the second most import organic building block in the chemical industry, is the starting material of many useful chemicals including polypropylene, propylene oxide, acrylonitrile, and butyraldehyde, which are the backbone of the modern polymer and pharmaceutical industry.[1-2] With the booming shale gas supplies, dehydrogenation of propane emerges as a promising technique to replace the current energy-intensive and low-yield petrochemical cracking of naphtha for propylene production.[3] In order to lower then energy consumption of this dehydrogenation technology, oxidative dehydrogenation of propane (ODHP) has been explored as an exothermic alternative. Although this lowers the thermodynamic barrier, it also causes over-oxidation of the desired propylene product.[4-5] Over the past decades, several ODHP catalysts have been developed, including VO_x, MoO_x, WO_x[6] and CrO_x[7] supported on silica,[8] zirconia,[9] alumina[10] and MOFs.[11] Despite the inspiring findings, it is still difficult for catalysts based on oxides to achieve high selectivity at moderate conversion due to lack of kinetic control in their catalytic nature.

Recently, borides were discovered to be a highly competitive alternative. Hexagonal boron nitride (hBN) in particular exhibited unexpectedly excellent catalytic performance towards ODHP, achieving 79% propene and 12% ethene at 14% propane conversion.[12] Furthermore, a broad family of borides, including Ti_2B, NiB, WB, HfB_2, Co_xB, hBN and B_4C, and even elemental boron, were reported to exhibit similarly high activity and selectivity towards ODHP.[13] It is clear that boron plays a key role in the ODHP catalysis, however, the structures of these B-containing catalytic interfaces in conditions of ODHP, the nature of the active site(s), and the catalytic mechanism remain elusive. So far, it has been found that B-O bonds are present on surfaces of spent catalysts, suggesting that a BO_x surface layer formed during the reaction. Such BO_x containing layer is highly likely to be the general catalytic surface for all ODHP boride catalysts.

In this work, we focus on the catalytic surface of hBN, perhaps the most interesting ODHP catalyst in the series, for that it is highly selective and active, consists of earth-abundant elements, and in the past was generally considered chemically inert.[14] We elucidate the structure of the hBN surface in the presence of oxygen and at the reaction temperature, using global optimization. A phase diagram as a function of the chemical potential of B and O (μ_B, μ_O) is constructed based on just the global optima, and then also based on the ensemble-average of all thermally-accessible structures. Electronic structure analysis is then performed for the whole ensemble, to reveal the special sites that emerge only in the reaction conditions. In addition, the dynamics of the interface is probed with ab initio molecular

dynamics (MD). We demonstrate that, in order to understand a catalytic surface under the realistic condition and evaluate the catalytic properties, it is necessary to account for the diversity and fluxionality of the dynamic interface at realistic conditions.

Since the presence of oxidized boron on the surface was suggested for all boride catalysis, we start by investigating how and if excess boron can bind to hBN. The particle-swarm global optimization (PSO) algorithm implemented in CALYPSO in combination with Density Functional Theory (DFT) calculations was applied to identify the hBN surface with varying boron coverage. The boron-rich surfaces are denoted as B_x ($x = 4\sim12$), with x being the number of excess B atoms added to the surface of the $2\times2\times1$ hBN supercell. The size of the unit cell is limited by the CALYPSO protocol, and the required amount of sampling. It is undoubtedly a constraint of the model: structures of the interface that could be accommodated in a larger supercell will not be discovered. However, we believe this does not qualitatively alter our conclusion regarding the structural diversity and the need for an ensemble representation of the surface in realistic conditions. The DFT calculations are performed using the Vienna ab-initio simulation package (VASP)[15] with the projector augmented wave (PAW)[16] and the PBE functional.[17] The D3 dispersion correction[18] was included. As is shown in **Figure S1**, B-B and B-N bonds are formed between excess boron and hBN surface, breaking the conjugated π-system of the top monolayer of hBN. With the coverage of B increasing, the structure of excess boron evolves from clusters to chains, interwoven networks, and finally an elemental boron layer with under-coordinated sides exposed.

In the oxygen atmosphere, the boron layer oxidizes. Using PSO-DFT, we next investigate the structure of the oxidized B-layer on top of the hBN surface with varying coverage of B and O atoms. The B, O-layers added to an $2\times2\times1$ supercell of hBN, are denoted as B_xO_y ($x = 4\sim6, y = 2\sim6$). The positions of the excess B and O atoms are sampled in the simulation, whereas the top of the hBN slab is allowed to relax in response to the changes in the oxide layer. As shown in **Figure S2**, the added oxygen readily inserts into the B-B bonds to form B-O-B, penetrates into the B layer, and further deforms the top hBN monolayer, suggesting the capability of boron-rich layer to activate oxygen. At higher O coverage, the surface becomes boron oxide-like, which is unfavorable for ODHP since boron oxide itself exhibits no activity.[10,11] The surfaces with moderate or relatively low O coverage are all possible candidates to do the catalysis.

To gain insight into the stability of those surface structures with different B and O coverage under realistic conditions, we calculate the surface free energy,

$$\gamma(T,p) = \frac{1}{A}[G_{\text{surface}}(T,p,N_i) - \sum N_i \mu_i(T,p)]$$

where A is the area of the surface unit cell, G_{surface} is the Gibbs free energy of the most stable surfaces for a specific stoichiometry, and μ is the chemical potential. Treating μ_{O} and μ_{B} as independent parameters, the chemical potential of B and O in bulk boron nitride, boron oxide and elemental boron are used as reference to compute γ based on the global optimum of each surface composition. Intersections of the γ for different surface stoichiometries splits the μ_{O} - μ_{B} plane into several regions, each dominated by a specific surface coverage of B and O, resulting in a surface phase diagram. It can be seen from that **Figure 1a** that, generally, increasing μ_{O} and μ_{B} leads to the stabilization of surfaces with higher coverage of O and B, respectively, indicating the drive toward the formation of the highly stable boron oxide layer. However, the change in the stoichiometry is not continuous with the change of the chemical potentials, due to instability of some phases such as B_6O_4, B_6O_5, and B_5O_6. Since μ_{O} in the realistic condition can be calculated by

$$\mu_{\text{O}}(T,p) = \mu^{\text{o}}(T,p^{\text{o}}) + \frac{1}{2}\, kT \ln(p/p^{o})$$

in which o superscript stands for standard conditions and p is the partial pressure of oxygen, a preliminary relationship can be established between reaction conditions and the surface composition of the catalyst (Table S1, SI). In the experiment, the pressures of oxygen tried so far have been between 250 and 150,000 Pa (and could me made higher),[12] and that range corresponds to a central portion of the phase diagrams show in Figure 1. Thus, our results provide a link between experimental conditions and specific surface structure, and therefore way to tune the conditions for a specific reactivity.

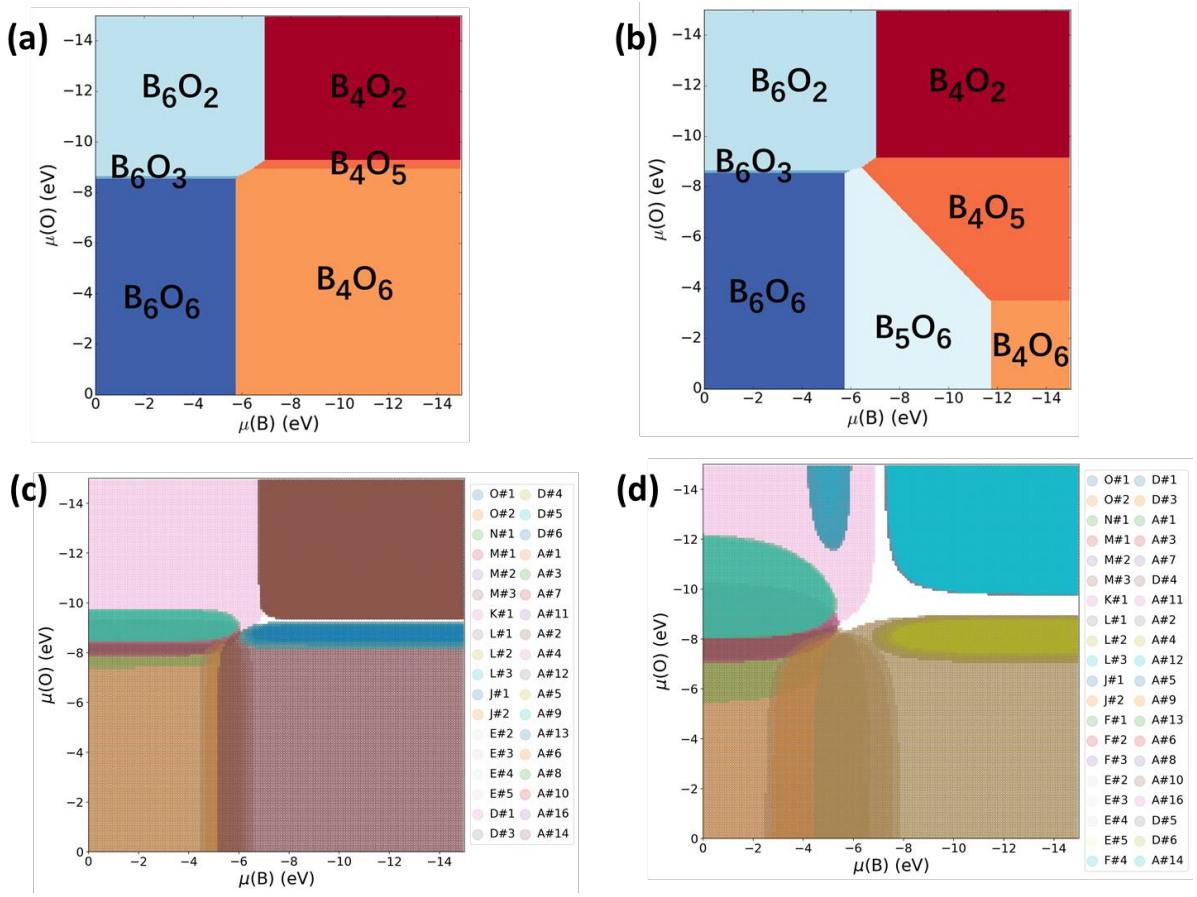

Figure 1. The surface phase diagram of B_xO_y on hBN as a function of μ_O and μ_B based on (a) the global optima only, (b) the ensemble average over all thermally-accessible minima of the same stoichiometry at 763 K, and the grand canonical ensemble representation at the population cutoff of > 5%, at (c) 298 K and (d) 763 K. Most of the fields of the grand canonical phase diagrams shown in (c) and (d) contain several colors corresponding to the accessible isomers of different stoichiometries in the ensemble (A, B, C, D, E, F, G, H, I, J, K, L, M, N, and O stand for B_4O_2, B_4O_3, B_4O_4, B_4O_5, B_4O_6, B_5O_2, B_5O_3, B_5O_4, B_5O_5, B_5O_6, B_6O_2, B_6O_3, B_6O_4, B_6O_5, and B_6O_6, respectively). The white fields represent areas where not a single isomer could be identified as leading.

However, the global optimization revealed that the under-stoichiometric BO surfaces have many competing structural isomers, whose relative energies should make them accessible at the temperature of ODHP. Several distinct isomers within 0.5 eV from global minimum for each surface composition were found, as shown in **Figure S2** (the n-th configuration counting from the global optimum of B_xO_y is referred to as B_xO_y#n). We observed in the past that for highly-dynamic catalytic interfaces, such as surface-supported sub-nano clusters, ensembles of many thermally-accessible states collectively define all catalyst properties, such as activity, selectivity, and stability.[19-18] Therefore, for each composition,

we constructed a statistical ensemble of surface states, with populations calculated by the Boltzmann statistics:

$$p_{\mathrm{i}} = \exp\left(-\frac{\varepsilon_i}{kT}\right) / \sum_i \exp\left(-\frac{\varepsilon_i}{kT}\right)$$

These populations are calculated at room temperature (298 K) and reaction temperature (763 K).[12] As T increases, metastable isomers get populated, while the contribution of the global optimum is reduced. It is important that the size for the accessible ensemble is stoichiometry-dependent, i.e. some compositions have one prominent global minimum even at 763 K, whereas other compositions are characterized by diverse ensembles of many states (**Table S2**). For example, B_6O_6 has just two accessible minima, whereas B_4O_2 has fifteen. As a result, phases rich in isomers become gradually destabilized at higher temperatures, due to the inclusion of higher-energy isomers in the ensemble. Hence, we reconstruct the surface phase diagram based on ensemble-averaged surface free energies, characteristic of the surface under at the realistic temperatures. As can been from **Figure 1b**, after including the local (metastable) minima, several phase boundaries shift, exposing previously inaccessible surface compositions, namely B_5O_6 and B_4O_5. The dramatic change in surface phase diagram strongly suggests that the chemistry of the interface might be greatly affected by the metastable isomers.

Taking the paradigm one step further, we allow the ensembles to not only populate alternative structural forms at higher T, but also change stoichiometry. In other words, we construct grand canonical ensembles, and build a phase diagrams in which different structures and different stoichiometries coexist within each field of μ_B and μ_O. The ε_i in the partition function is substituted with the γ, allowing us to calculate the population distribution of each surface structure. As the temperature is elevated to 298 K (**Figure 1c**), some isomers of different stoichiometries get populated and appear in each field on the phase diagram. At 763 K (**Figure 1d**) the dominance of the global minima is reduced significantly more than when a fixed stoichiometry was considered. Some areas on the phase diagram (depicted in white in **Figure 1c,d**) lack any leading configuration in the ensemble, indicating that the surface would pay a minimal energetic penalty for reorganization and changes in composition. This potentially indicates that, in these areas of μ_B and μ_O, the exchange of oxygen atoms between the surface, the gas phase, and the reacting system should be particularly easy.

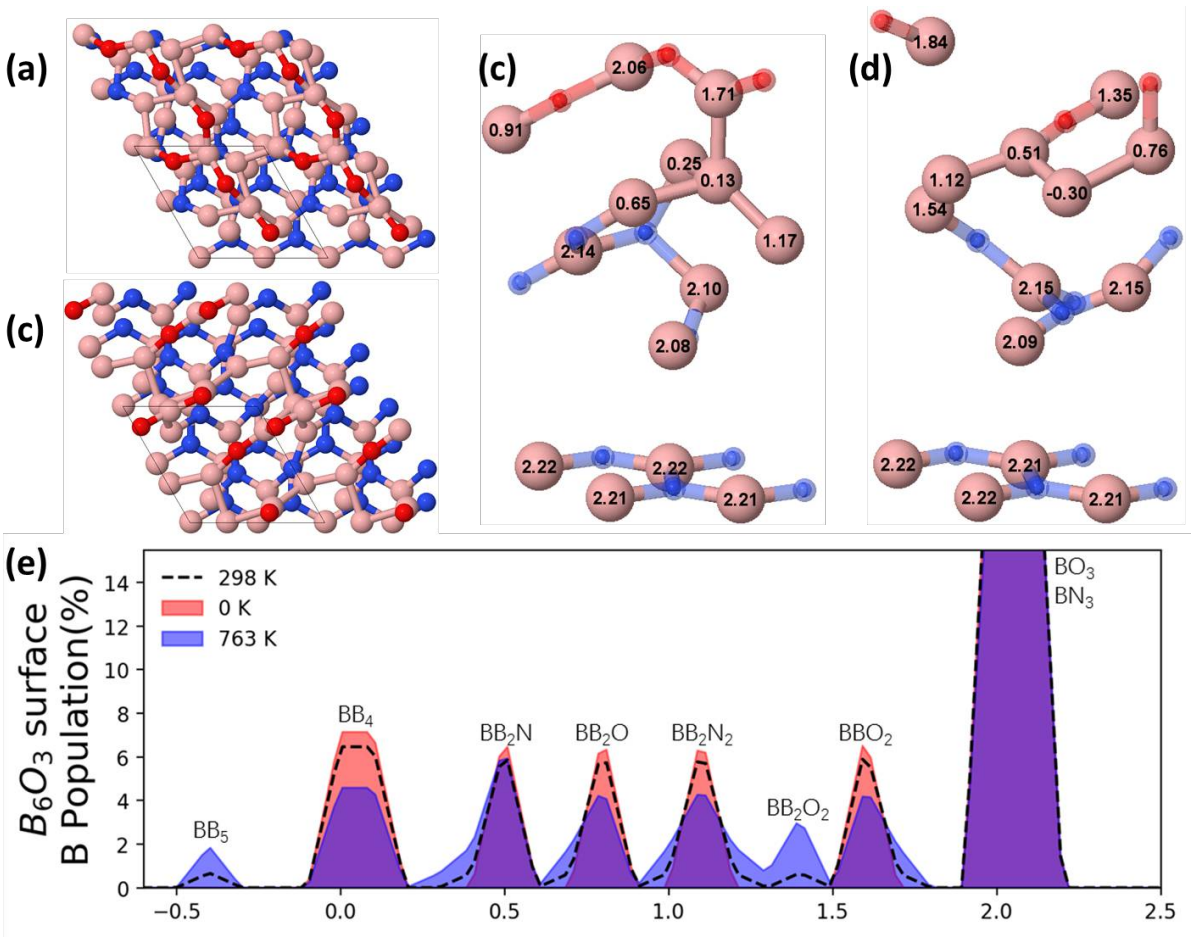

Figure 2. The structure of (a) B_6O_3#1 and (b) B_6O_3#2 shown in a $2\times2\times1$ supercell. Calculated Bader charge of boron atoms labeled in unit cells of (c) B_6O_3#1 and (d) B_6O_3#2. Pink, red and blue balls represent boron, oxygen and nitrogen, respectively. N and O atoms are set transparent in (c) and (d) for clarity of Bader charge labels. (e) shows the ensemble-averaged Bader charge distribution of B_6O_3 at temperature of 0 K, 298 K and 763 K, with x axis being Bader charge value.

The electronic structure of the interface should reflect the found geometric and compositional changes, impacting the potential catalytic mechanism. Indeed, the impressive difference between the phase diagrams based on statistical ensembles and global optima also calls for an ensemble-averaged view on the catalytic activity. Due to the structural diversity of the isomers in the ensemble it is extremely computationally expensive to explore the ODHP reaction mechanism for all surface structures and possible sites. To begin unraveling this complexity, we performed the electronic structure analysis of the found phases. We calculated the Bader charges on boron atoms in all the surface structures contributing to the phase diagram as a function of *T*. Stoichiometric boron oxide exhibits no activity toward ODHP, while elemental boron shows the best performance. Bader charges

of B in elemental boron, boron oxide and boron nitride were calculated to be c.a. 0, +2.2 and +2.2, respectively. In the found isomers, B atoms are positioned in diverse chemical environments and have different Bader charge. For example, a B atom coordinated to another B and to N, as in B-B-N, has a Bader charge of c.a. +0.9, and the value increases to c.a. +1.3 when O or N is added, while decreases to c.a. +0.6 when another B is added. Strain and the second coordination sphere in the chemical environment of an atom also affect the atomic charge. We constructed the statistical distributions of Bader charges to distinguish different types of B atoms present at varying conditions, and to understand their contribution to overall chemical properties. Ensemble-averaged Bader charge distribution at different temperatures (**Figure S3**) reflect how the apparent electronic structure of the interface changes when metastable isomers get populated, which may assist the search for chemically interesting sites responsible for catalysis. In the range of charge from -0.5 to +2.2 (as in BN), 2-7 different charge states of B are present on the surface, depending on the stoichiometry. The effect of increasing *T* mostly consists of broadening of the peaks, i.e. subtly changing the charge distributions within the same typical coordination environments. Expectedly, stoichiometries that exhibit greater population sizes, and hence greater electronic structure diversity (e.g. B_4O_2, B_4O_3, B_5O_4, B_6O_3, B_6O_5) also have the highest sensitivity of the electronic structure to rising *T*. On the other hand, stoichiometries such as B_6O_2 remain indifferent to *T* rise in terms of the apparent electronic structure. Intuitively, it is more likely that less stable sites are more reactive. Therefore, it is possible that those special charge states on B that develop at rising *T* are the ones important for the catalytic mechanism. Given that elemental B is the best catalyst for ODHP, and that B atoms in the coordination environments like in elemental B apparently emerge in conditions of ODHP, at least in simulations, we can speculate that these sites are the most relevant to catalysis. Several such sites exist on the surfaces of some stoichiometries in our simulations (**Figure S3**), and in B_4O_2 and B_4O_5, the populations of low-charge states grow with rising *T*. The unusual -0.5 charge state appears in B_6O_2 and B_6O_3, and it corresponds to the coordination sphere consisting of BB_5.

Finally, *ab intio* MD simulation provides some insight into whether or not the various structural isomers of the interface are kinetically accessible and gave structural information on the species that transiently form on the surface. The NVT ensemble at 763 K with the Nose-Hoover thermostat was used. 50 ps trajectories with the time step of 1 fs were performed. Images were collected every 50 fs after the system was equilibrated. We found that isomers with same chemical composition can behave very differently in MD. For some isomers, such as B_6O_6#2, the B, O-layer stays stable over the duration of the simulation, showing no bond dissociation or any reconstructing (**Figure 3a**). This can

be attributed to the structural similarity of this interface with boron oxide, where most of the B atoms are saturated by the stable B-O bonds. However, some other isomers exhibited very different properties. B_6O_6#1 detached from the hBN surface during MD and reconstructed into a layer with high fluxionality (**Figure 3b**). Some boron atoms come together to form dynamical arrangements containing usually unstable units, such as -B=O and B_2O cycles. At lower oxygen coverage, such units can become more prevalent and stable, for example in B_6O_3#2 (**Figure 3c**). Inspired by the previously reported catalytic activity of -B=O in other systems and the B_2O cycle which is interesting in terms of its 3-center bonding nature, we further study those units by calculating Bader charge and structural parameters.[20-21] Bader charge analysis shows that the atomic charge of O is c.a. -1.40 in -B=O and c.a. -1.50 in B_2O cycles, which differs from the value in the boron oxide (c.a. -1.57). Knowing that boron oxide is not catalytic for ODH, the less negative Bader charge of O suggests a possibility of C-H activation reactivity on these special sites. In B_2O cycle, an O atom bridges two B atoms, and the bridging B-O has a length of c.a. 1.5 Å which is markedly longer than B-O in boron oxide (c.a. 1.3 Å), suggesting a weaker bond strength and higher structural flexibility. Hence, these transient units, with electronic structures different from boron oxide, are also candidate active sites. It is possible that the catalysis is due to the dynamical layer that forms *in-situ*, featuring reactive units unavailable in stable isomers, and the activity difference between the borides lies in their ability to generate a significant population of such a dynamical layer. We are still far from a clear conclusion, but the possibility definitely deserves awareness.

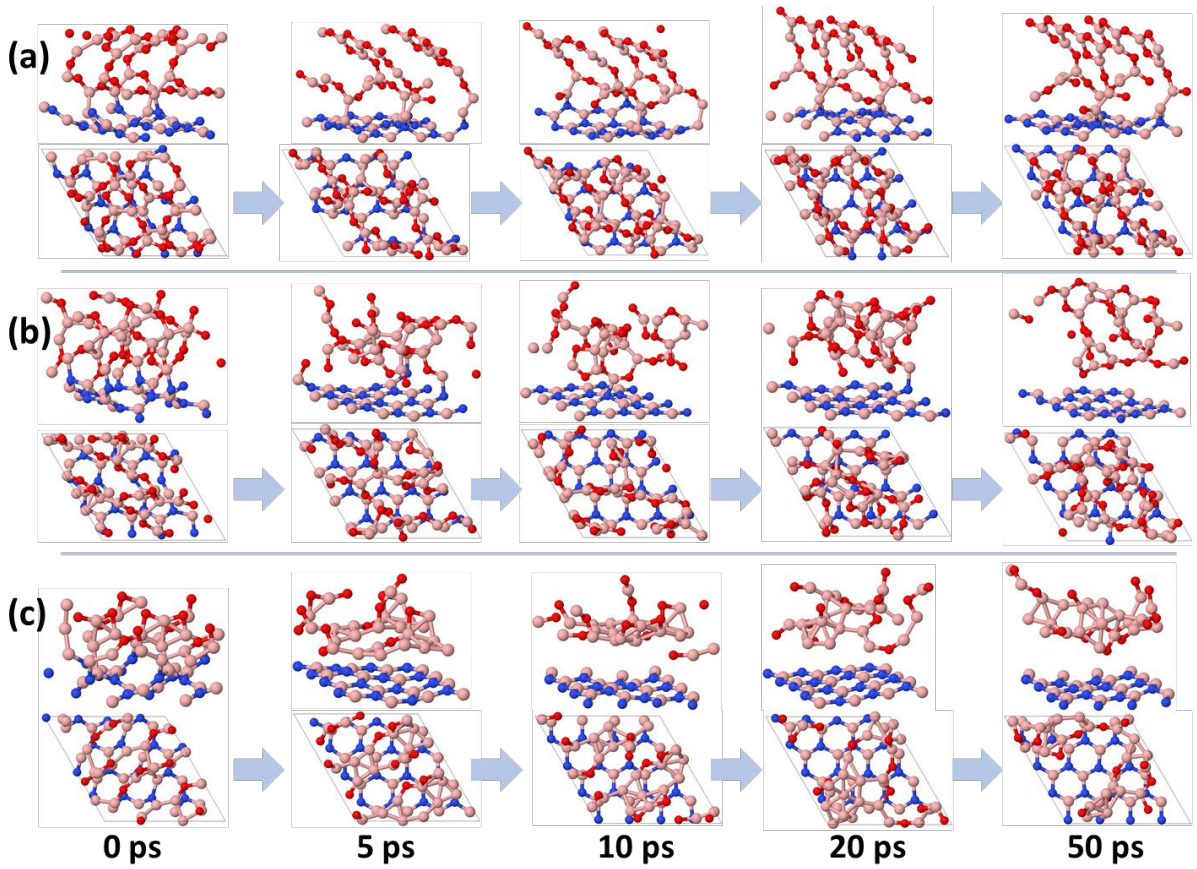

Figure 3. *ab initio* MD simulation results of (a) B_6O_6#2 and (b) B_6O_6#1, and (c) B_6O_3#2 with duration of 50 ps. Bulk hBN layers are emitted for clarity of the surface region.

In summary, we predicted the structures of hBN surface layer with different coverage of B and O via PSO-DFT global optimization and obtained structurally diverse low energy isomers for each surface composition. Surface phase diagram, with respect to chemical potential of B and O, was established based on the global minima (i.e. at 0 K), the canonical ensemble, and the grand canonical ensemble, to evaluate the stability of surfaces with different composition at increasing temperature. We showed how including contributions of low-energy metastable isomers dramatically alters the phase diagram. We thus demonstrate the necessity of ensemble-averaging in representing a catalytic surface in realistic conditions of catalysis. Bader charge distributions under different temperatures were calculated to further investigate the evolution of the electronic structure of the interface at rising *T*, possibly guiding the search for active sites in the future. Additionally, dynamical layer with exposed -B=O units were discovered on surface with lower O coverage via MD simulation, providing a new dimension to discover transient active sites in catalysis. Though turning to a statistical ensemble brings a much

greater complexity, both in characterization and in computation, the ensemble representation is bound to be the key to access a new domain of chemistry.

Supporting Information Available. Full computational details, slab models for global optimization and μ calculation, structure of global minima of boron-rich hBN surfaces, structure of accessible isomers of B_xO_y surfaces, ensemble-averaged Bader charge distribution of boron in B_xO_y surfaces, μ_O in different T, p, and number of accessible isomers of different stoichiometries at reaction T.

Acknowledgements. This work was supported by the NSF CAREER Award (CHE-1351968) to A.N.A.. Z.Z. was supported by the CSST Summer Fellowship. E.J.I. acknowledges the Postdoctoral Fellowship of the Basque Country (POS 2015 1 0008). Extreme Science and Engineering Discovery Environment's (XSEDE) computing resources, UCLA-IDRE cluster, and SUSTech HPC cluster were used to conduct this work.

References

(1) *Market Study: Propylene, 2nd ed.* Ceresana: http://www.ceresana.com/en/market-studies/chemicals/propylene/; 2014.
(2) Plotkin, J. S. The Changing Dynamics of Olefin Supply/demand. *Catal. Today* **2005**, *106*, 10-14.
(3) Cavani, F.; Ballarini, N.; Cericola, A. Oxidative Dehydrogenation of Ethane and Propane: How Far From Commercial Implementation? *Catal. Today* **2007**, *127*, 113-131.
(4) Gong, C. M.; Ning, H. B.; Xu, J. Q.; Li, Z. R.; Zhu, Q.; Li, X. Y. Experimental and Modeling Study of Thermal and Catalytic Cracking of n-decane. *J. Anal. Appl. Pyrolysis* **2014**, *110*, 463-469.
(5) Kung, H. H. Oxidative Dehydrogenation of Light (C2 to C4) Alkanes. *Adv. Catal.* **1994**, *40*, 1-38.
(6) Chen, K.; Bell, A. T.; Iglesia, E. Kinetics and Mechanism of Oxidative Dehydrogenation of Propane on Vanadium, Molybdenum, and Tungsten Oxides. *J. Phys. Chem. B* **2000**, *104*, 1292-1299.
(7) Cherian, M.; Rao, M. S.; Hirt, A. M.; Wachs, I. E.; Deo, G. Oxidative Dehydrogenation of Propane over Supported Chromia Catalysts: Influence of Oxide Supports and Chromia Loading. *J. Catal.* **2002**, *211*, 482-495.
(8) Dinse, A.; Khennache, S.; Frank, B.; Hess, C.; Herbert, R.; Wrabetz, S.; Schlögl, R.; Schomäcker, R. Oxidative Dehydrogenation of Propane on Silica (SBA-15) Supported Vanadia Catalysts: A Kinetic Investigation. *J. Mol. Catal. A: Chem.* **2009**, *307*, 43-50.
(9) Otroshchenko, T.; Sokolov, S.; Stoyanova, M.; Kondratenko, V. A.; Rodemerck, U.; Linke, D.; Kondratenko, E. V. ZrO2-Based Alternatives to Conventional Propane Dehydrogenation Catalysts: Active Sites, Design, and Performance. *Angew. Chem. Int. Ed.* **2015**, *54*, 15880-15883.
(10) Argyle, M. D.; Chen, K.; Bell, A. T.; Iglesia, E. Effect of Catalyst Structure on Oxidative Dehydrogenation of Ethane and Propane on Alumina-Supported Vanadia. *J. Catal.* **2002**, *208*, 139-149.
(11) Li, Z.; Peters, A. W.; Bernales, V.; Ortuño, M. A.; Schweitzer, N. M.; DeStefano, M. R.; Gallington, L. C.; Platero-Prats, A. E.; Chapman, K. W.; Cramer, C. J., et al. Metal–Organic

Framework Supported Cobalt Catalysts for the Oxidative Dehydrogenation of Propane at Low Temperature. *ACS Cent. Sci.* **2017**, *3*, 31-38.
(12) Grant, J. T.; Carrero, C. A.; Goeltl, F.; Venegas, J.; Mueller, P.; Burt, S. P.; Specht, S. E.; McDermott, W. P.; Chieregato, A.; Hermans, I. Selective Oxidative Dehydrogenation of Propane to Propene using Boron Nitride Catalysts. *Science* **2016**, *354*, 1570-1573.
(13) Grant, J. T.; McDermott, W. P.; Venegas, J. M.; Burt, S. P.; Micka, J.; Phivilay, S. P.; Carrero, C. A.; Hermans, I. Boron and Boron-Containing Catalysts for the Oxidative Dehydrogenation of Propane. *ChemCatChem* **2017**, *9*, 3623-3626.
(14) Shi, L.; Wang, Y.; Yan, B.; Song, W.; Shao, D.; Lu, A.-H. Progress in Selective Oxidative Dehydrogenation of Light Alkanes to Olefins Promoted by Boron Nitride Catalysts. *Chem. Commun.* **2018**, *54*, 10936-10946.
(15) Kresse, G.; Furthmuller, J. Efficient Iterative Schemes for ab initio Total-energy Calculations Using a Plane-wave Basis Set. *Phys. Rev. B* **1996**, *54*, 11169-11186.
(16) Blöchl, P. E. Projector Augmented-wave Method. *Phys. Rev. B* **1994**, *50*, 17953–17979.
(17) Perdew, J. P.; Burke, K.; Ernzerhof, M. Generalized Gradient Approximation Made Simple. *Phys. Rev. Lett.* **1996**, *77*, 3865-3868.
(18) Grimme, S.; Antony, J.; Ehrlich, S.; Krieg, H. A Consistent and Accurate ab initio Parametrization of Density Functional Dispersion Correction (DFT-D) for the 94 Elements H-Pu. *J. Chem. Phys.* **2010**, *132*, 154104.
(19) Zhai, H.; Alexandrova, A. N. Fluxionality of Catalytic Clusters: When It Matters and How to Address It. *ACS Catal.* **2017**, *7*, 1905-1911.
(20) Braunschweig, H.; Radacki, K.; Schneider, A. Oxoboryl Complexes: Boron−Oxygen Triple Bonds Stabilized in the Coordination Sphere of Platinum. *Science* **2010**, *328*, 345-347.
(21) Braunschweig, H.; Radacki, K.; Schneider, A. Cyclodimerization of an Oxoboryl Complex Induced by trans Ligand Abstraction. *Angew. Chem. Int. Ed.* **2010**, *49*, 5993-5996.

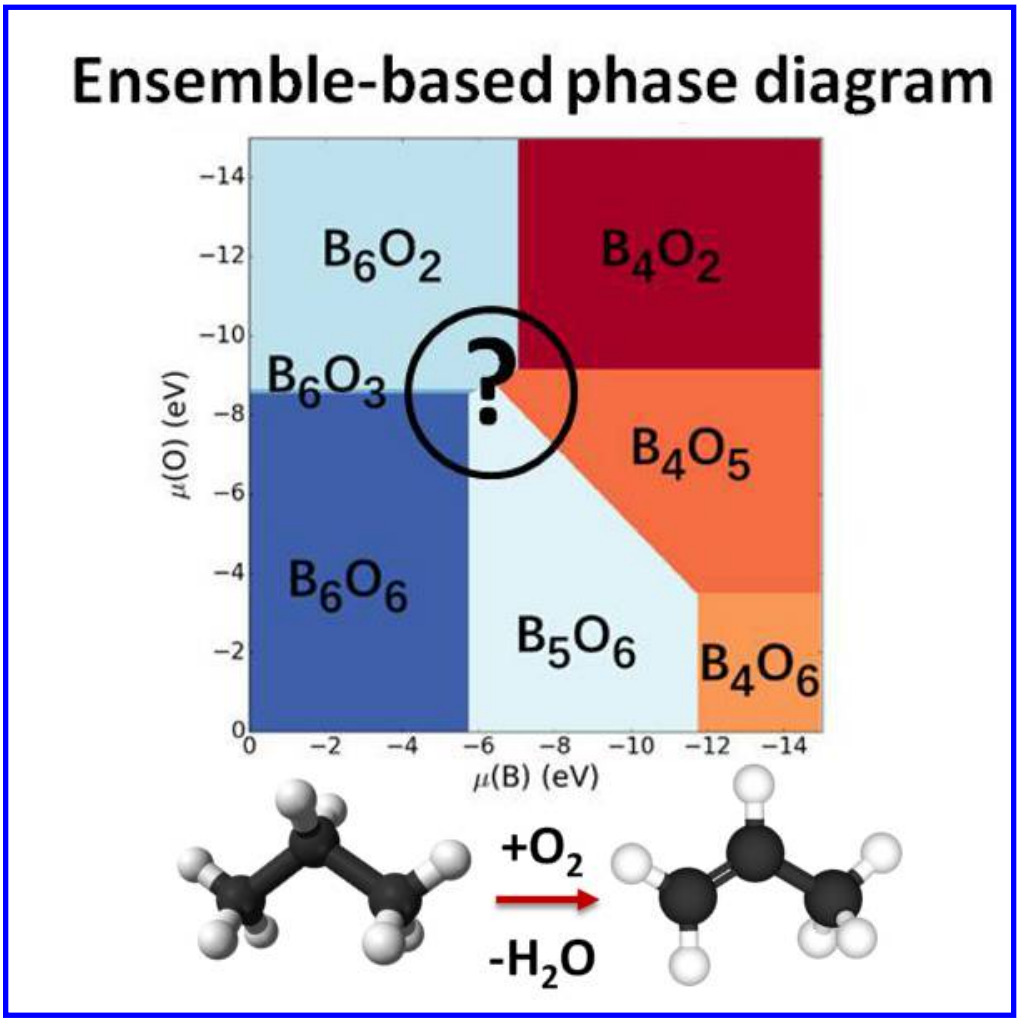

50x50mm (300 x 300 DPI)

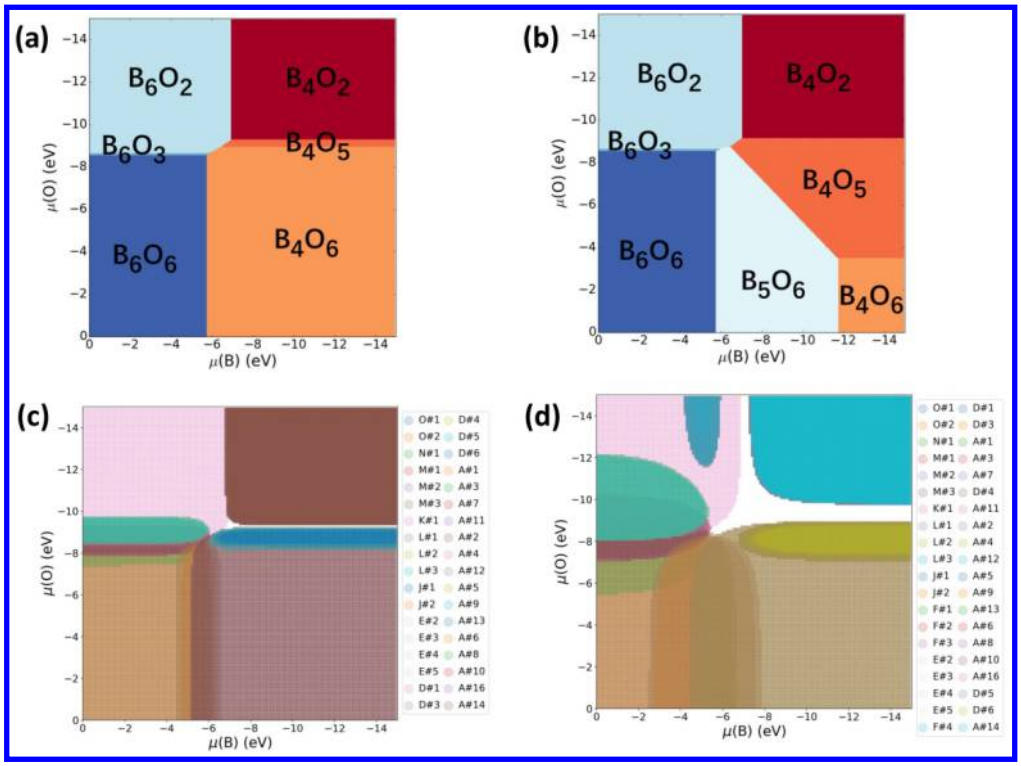

678x503mm (72 x 72 DPI)

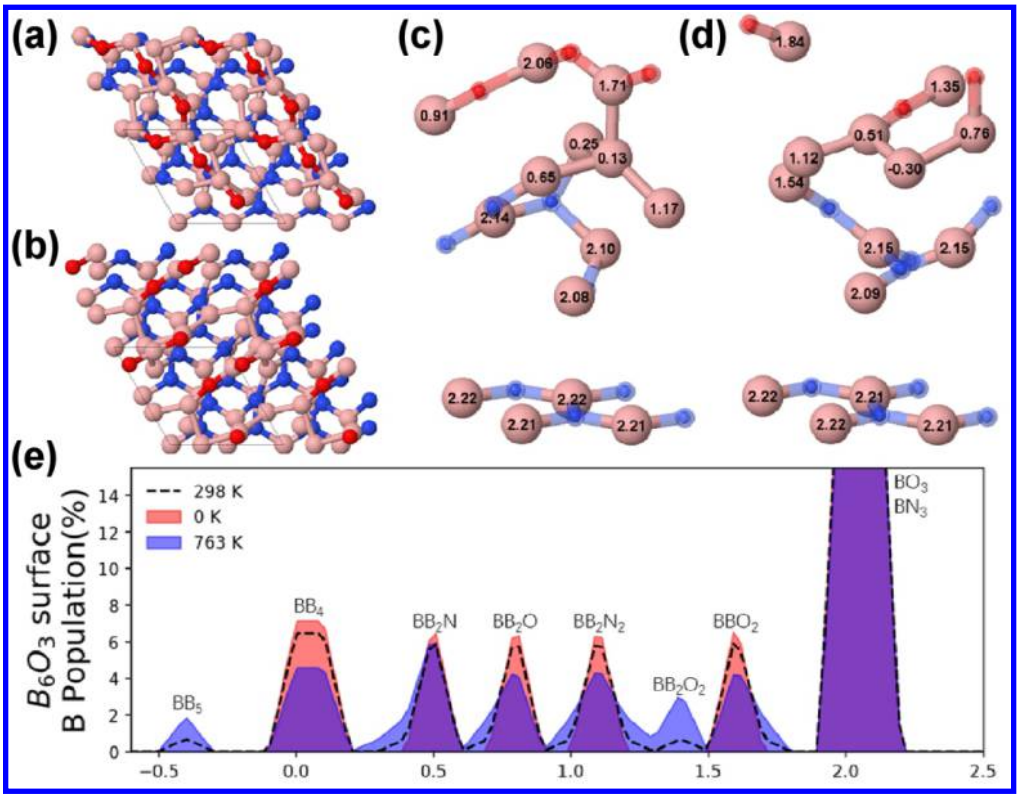

493x382mm (72 x 72 DPI)

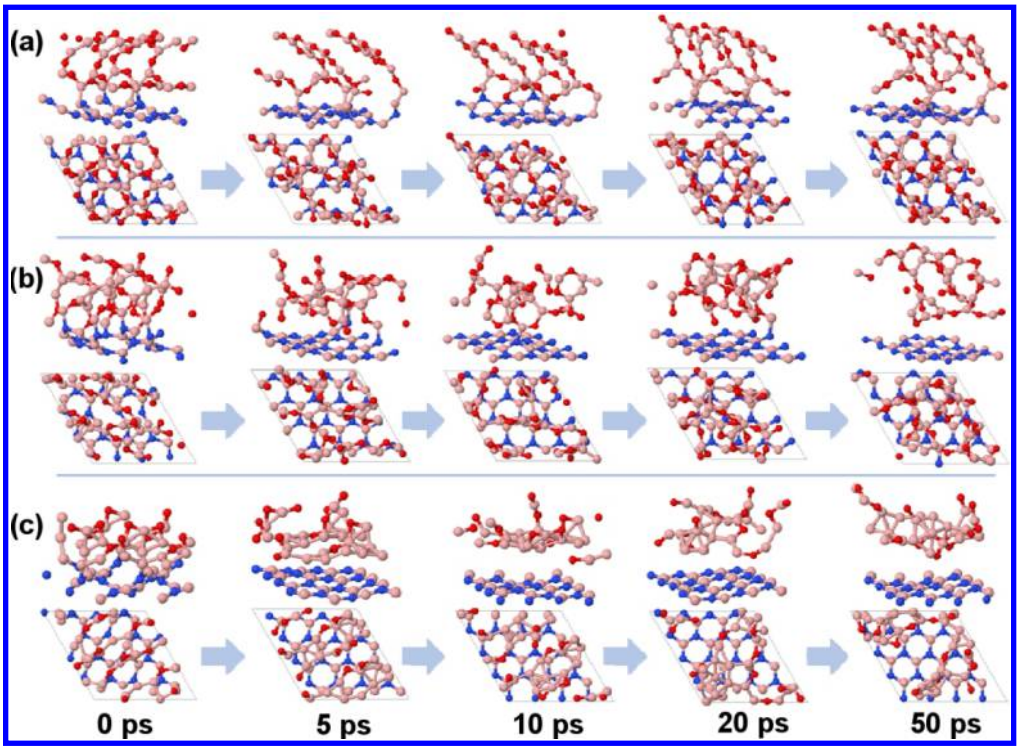

491x357mm (72 x 72 DPI)